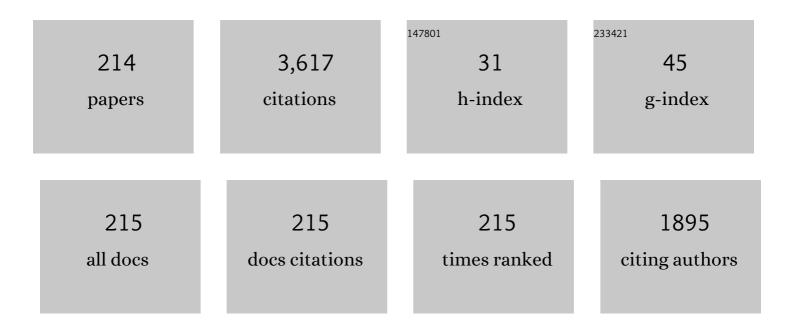
List of Publications by Year in descending order

Source: https://exaly.com/author-pdf/6079657/publications.pdf Version: 2024-02-01



Τοριι Πιιμαρα

#	Article	IF	CITATIONS
1	Grain growth behaviors of polycrystalline silicon during melt growth processes. Journal of Crystal Growth, 2004, 266, 441-448.	1.5	101
2	Enhanced quantum efficiency of solar cells with self-assembled Ge dots stacked in multilayer structure. Applied Physics Letters, 2003, 83, 1258-1260.	3.3	99
3	In situ observation of elementary growth steps on the surface of protein crystals by laser confocal microscopy. Journal of Crystal Growth, 2004, 262, 536-542.	1.5	98
4	Lipid Bilayer Membrane with Atomic Step Structure: Supported Bilayer on a Step-and-Terrace TiO ₂ (100) Surface. Langmuir, 2008, 24, 11567-11576.	3.5	76
5	In situ observations of crystal growth behavior of silicon melt. Journal of Crystal Growth, 2002, 243, 275-282.	1.5	71
6	In-situ observations of melt growth behavior of polycrystalline silicon. Journal of Crystal Growth, 2004, 262, 124-129.	1.5	69
7	Super-High Brightness and High-Spin-Polarization Photocathode. Applied Physics Express, 0, 1, 045002.	2.4	68
8	High-Efficiency Conversion of Threading Screw Dislocations in 4H-SiC by Solution Growth. Applied Physics Express, 2012, 5, 115501.	2.4	67
9	Minority carrier lifetime in polycrystalline silicon solar cells studied by photoassisted Kelvin probe force microscopy. Applied Physics Letters, 2008, 93, .	3.3	64
10	Top-seeded solution growth of three-inch-diameter 4H-SiC using convection control technique. Journal of Crystal Growth, 2014, 395, 68-73.	1.5	59
11	Growth rate and surface morphology of 4H–SiC crystals grown from Si–Cr–C and Si–Cr–Al–C solutions under various temperature gradient conditions. Journal of Crystal Growth, 2014, 401, 681-685.	1.5	58
12	In situ growth of superconducting NdFeAs(O,F) thin films by molecular beam epitaxy. Applied Physics Letters, 2010, 97, 042509.	3.3	57
13	Epitaxial Growth of NdFeAsO Thin Films by Molecular Beam Epitaxy. Applied Physics Express, 2009, 2, 093002.	2.4	52
14	30-kV spin-polarized transmission electron microscope with GaAs–GaAsP strained superlattice photocathode. Applied Physics Letters, 2012, 101, .	3.3	52
15	Kinetic analysis of spinodal decomposition process in Fe–Cr alloys by small angle neutron scattering. Acta Materialia, 2000, 48, 1629-1637.	7.9	51
16	Low-dislocation-density 4H-SiC crystal growth utilizing dislocation conversion during solution method. Applied Physics Express, 2014, 7, 065501.	2.4	51
17	Evolution of threading screw dislocation conversion during solution growth of 4H-SiC. APL Materials, 2013, 1, .	5.1	50
18	Growth of SiGe bulk crystal with uniform composition by directly controlling the growth temperature at the crystal–melt interface using in situ monitoring system. Journal of Crystal Growth, 2001, 224, 204-211.	1.5	49

#	Article	IF	CITATIONS
19	High brightness and high polarization electron source using transmission photocathode with GaAs-GaAsP superlattice layers. Journal of Applied Physics, 2008, 103, .	2.5	49
20	High-speed prediction of computational fluid dynamics simulation in crystal growth. CrystEngComm, 2018, 20, 6546-6550.	2.6	48
21	Effect of aluminum addition on the surface step morphology of 4H–SiC grown from Si–Cr–C solution. Journal of Crystal Growth, 2015, 423, 45-49.	1.5	45
22	Real Time Magnetic Imaging by Spin-Polarized Low Energy Electron Microscopy with Highly Spin-Polarized and High Brightness Electron Gun. Applied Physics Express, 2010, 3, 026601.	2.4	41
23	Solution Growth of SiC Crystal with High Growth Rate Using Accelerated Crucible Rotation Technique. Materials Science Forum, 2006, 527-529, 119-122.	0.3	38
24	Critical current density and grain boundary property of BaFe2(As,P)2 thin films. Physica C: Superconductivity and Its Applications, 2013, 494, 181-184.	1.2	38
25	Coherence of a spin-polarized electron beam emitted from a semiconductor photocathode in a transmission electron microscope. Applied Physics Letters, 2014, 105, .	3.3	38
26	Photovoltage Mapping on Polycrystalline Silicon Solar Cells by Kelvin Probe Force Microscopy with Piezoresistive Cantilever. Japanese Journal of Applied Physics, 2007, 46, 5548.	1.5	37
27	Compositional variation in Si-rich SiGe single crystals grown by multi-component zone melting method using Si seed and source crystals. Journal of Crystal Growth, 2002, 240, 373-381.	1.5	35
28	Influence of Solution Flow on Step Bunching in Solution Growth of SiC Crystals. Crystal Growth and Design, 2013, 13, 3691-3696.	3.0	35
29	Different behavior of threading edge dislocation conversion during the solution growth of 4H–SiC depending on the Burgers vector. Acta Materialia, 2014, 81, 284-290.	7.9	34
30	Thermal emittance measurements for electron beams produced from bulk and superlattice negative electron affinity photocathodes. Journal of Applied Physics, 2007, 102, 024904.	2.5	33
31	Anomalous Diffusion in Supported Lipid Bilayers Induced by Oxide Surface Nanostructures. Langmuir, 2011, 27, 9662-9665.	3.5	33
32	Conversion Mechanism of Threading Screw Dislocation during SiC Solution Growth. Materials Science Forum, 0, 717-720, 351-354.	0.3	33
33	Ge composition dependence of properties of solar cells based on multicrystalline SiGe with microscopic compositional distribution. Journal of Applied Physics, 2004, 96, 1238-1241.	2.5	32
34	Solution growth of high-quality 3C-SiC crystals. Journal of Crystal Growth, 2008, 310, 1438-1442.	1.5	32
35	Molecular Beam Epitaxy Growth of Superconducting NdFeAs(O,F) Thin Films Using a F-Getter and a Novel F-Doping Method. Applied Physics Express, 2011, 4, 083102.	2.4	32
36	Nitrogen doping of 4H–SiC by the top-seeded solution growth technique using Si–Ti solvent. Journal of Crystal Growth, 2014, 392, 60-65.	1.5	32

#	Article	IF	CITATIONS
37	The Boersch effect in a picosecond pulsed electron beam emitted from a semiconductor photocathode. Applied Physics Letters, 2016, 109, .	3.3	32
38	Effects of misfit dislocations and AlN buffer layer on the GaInN/GaN phase diagram of the growth mode. Journal of Applied Physics, 2001, 89, 146-153.	2.5	31
39	Growth of SiGe bulk crystals with uniform composition by utilizing feedback control system of the crystal–melt interface position for precise control of the growth temperature. Journal of Crystal Growth, 2003, 250, 298-304.	1.5	30
40	Solution Growth of Self-Standing 6H-SiC Single Crystal Using Metal Solvent. Materials Science Forum, 2004, 457-460, 123-126.	0.3	30
41	Polytype Transformation by Replication of Stacking Faults Formed by Two-Dimensional Nucleation on Spiral Steps during SiC Solution Growth. Crystal Growth and Design, 2012, 12, 3209-3214.	3.0	30
42	Global simulation of the induction heating TSSG process of SiC for the effects of Marangoni convection, free surface deformation and seed rotation. Journal of Crystal Growth, 2017, 470, 75-88.	1.5	29
43	Crystal quality of a 6H-SiC layer grown over macrodefects by liquid-phase epitaxy: a Raman spectroscopic study. Thin Solid Films, 2005, 476, 206-209.	1.8	27
44	Enantioselective amplification on circularly polarized laser-induced chiral nucleation from a NaClO ₃ solution containing Ag nanoparticles. CrystEngComm, 2016, 18, 7441-7448.	2.6	27
45	Achiral Metastable Crystals of Sodium Chlorate Forming Prior to Chiral Crystals in Solution Growth. Crystal Growth and Design, 2013, 13, 5188-5192.	3.0	26
46	The strain effect on the superconducting properties of BaFe ₂ (As, P) ₂ thin films grown by molecular beam epitaxy. Superconductor Science and Technology, 2014, 27, 065005.	3.5	26
47	Non-uniform electrodeposition of zinc on the (0001) plane. Thin Solid Films, 2015, 590, 207-213.	1.8	26
48	Substrate dependence of the superconducting properties of NdFeAs(O,F) thin films. Solid State Communications, 2012, 152, 735-739.	1.9	25
49	Highly spin-polarized electron photocathode based on GaAs–GaAsP superlattice grown on mosaic-structured buffer layer. Journal of Crystal Growth, 2008, 310, 5039-5043.	1.5	24
50	Effect of Crystal Orientation of Cu Current Collectors on Cycling Stability of Li Metal Anodes. ACS Applied Materials & Interfaces, 2020, 12, 9341-9346.	8.0	24
51	Magnetic Damping of the Temperature-Driven Convection in NaCl Aqueous Solution Using a Static and Homogeneous Field of 10 T. Japanese Journal of Applied Physics, 1999, 38, L842-L844.	1.5	22
52	Effects of high pressure on the growth kinetics of orthorhombic lysozyme crystals. Journal of Crystal Growth, 2003, 254, 188-195.	1.5	22
53	Effects of spacer thickness on quantum efficiency of the solar cells with embedded Ge islands in the intrinsic layer. Applied Physics Letters, 2004, 84, 2802-2804.	3.3	22
54	Reduction of Threading Screw Dislocation Utilizing Defect Conversion during Solution Growth of 4H-SiC. Materials Science Forum, 0, 740-742, 189-192.	0.3	22

#	Article	IF	CITATIONS
55	Adaptive process control for crystal growth using machine learning for high-speed prediction: application to SiC solution growth. CrystEngComm, 2021, 23, 1982-1990.	2.6	22
56	On the origin of strain fluctuation in strained-Si grown on SiGe-on-insulator and SiGe virtual substrates. Applied Physics Letters, 2004, 85, 1335-1337.	3.3	21
57	Crystalline Quality Evaluation of 6H-SiC Bulk Crystals Grown from Si-Ti-C Ternary Solution. Materials Science Forum, 2005, 483-485, 13-16.	0.3	21
58	Formation process of 3C-SiC on 6H-SiC (0001) by low-temperature solution growth in Si–Sc–C system. Journal of Crystal Growth, 2011, 335, 94-99.	1.5	21
59	Conversion Behavior of Threading Screw Dislocations on C Face with Different Surface Morphology During 4H-SiC Solution Growth. Crystal Growth and Design, 2016, 16, 6436-6439.	3.0	21
60	Crystal Orientation Dependence of Precipitate Structure of Electrodeposited Li Metal on Cu Current Collectors. Crystal Growth and Design, 2017, 17, 2379-2385.	3.0	21
61	Modification of the surface morphology of 4H-SiC by addition of Sn and Al in solution growth with SiCr solvents. Journal of Crystal Growth, 2017, 458, 37-43.	1.5	21
62	Epitaxial relation and island growth of perylene-3.4.9.10-tetracarboxylic dianhydride (PTCDA) thin film crystals on a hydrogen-terminated Si(111) substrate. Journal of Crystal Growth, 2004, 262, 196-201.	1.5	20
63	High-quality and large-area 3C–SiC growth on 6H–SiC(0 0 0 1) seed crystal with top-seeded solution method. Journal of Crystal Growth, 2011, 318, 389-393.	1.5	20
64	Polytype-selective growth of SiC by supersaturation control in solution growth. Journal of Crystal Growth, 2012, 360, 176-180.	1.5	20
65	Bayesian optimization for a high- and uniform-crystal growth rate in the top-seeded solution growth process of silicon carbide under applied magnetic field and seed rotation. Journal of Crystal Growth, 2020, 532, 125437.	1.5	20
66	Geometrical design of a crystal growth system guided by a machine learning algorithm. CrystEngComm, 2021, 23, 2695-2702.	2.6	20
67	Physical model for the evaluation of solid–liquid interfacial tension in silicon. Journal of Applied Physics, 2001, 90, 750-755.	2.5	19
68	Influence of the elastic strain on the band structure of ellipsoidal SiGe coherently embedded in the Si matrix. Journal of Applied Physics, 2003, 94, 916-920.	2.5	19
69	Study of minority carrier diffusion length in multicrystalline silicon solar cells using photoassisted Kelvin probe force microscopy. Applied Physics Letters, 2009, 95, 191908.	3.3	19
70	Emergence and Amplification of Chirality via Achiral–Chiral Polymorphic Transformation in Sodium Chlorate Solution Growth. Crystal Growth and Design, 2014, 14, 3596-3602.	3.0	19
71	Two-step SiC solution growth for dislocation reduction. Journal of Crystal Growth, 2017, 468, 874-878.	1.5	19
72	Intensity Interference in a Coherent Spin-Polarized Electron Beam. Physical Review Letters, 2021, 126, 125501.	7.8	19

#	Article	IF	CITATIONS
73	New method for measurement of interdiffusion coefficient in high temperature solutions based on Fick's first law. Journal of Crystal Growth, 2002, 241, 387-394.	1.5	18
74	Top-Seeded Solution Growth of 3 Inch Diameter 4H-SiC Bulk Crystal Using Metal Solvents. Materials Science Forum, 0, 778-780, 79-82.	0.3	18
75	Melt growth of multicrystalline SiGe with large compositional distribution for new solar cell applications. Solar Energy Materials and Solar Cells, 2002, 72, 93-100.	6.2	17
76	Analysis of the carbon transport near the growth interface with respect to the rotational speed of the seed crystal during top-seeded solution growth of SiC. Japanese Journal of Applied Physics, 2016, 55, 125601.	1.5	17
77	Growth and properties of SiGe multicrystals with microscopic compositional distribution for high-efficiency solar cells. Solar Energy Materials and Solar Cells, 2002, 73, 305-320.	6.2	16
78	A simple approach to determine preferential growth orientation using multiple seed crystals with random orientations and its utilization for seed optimization to restrain polycrystallization of SiGe bulk crystal. Journal of Crystal Growth, 2005, 276, 393-400.	1.5	16
79	Photovoltage Mapping on Polycrystalline Silicon Solar Cells through Potential Measurements by Atomic Force Microscopy with Piezoresistive Cantilever. Japanese Journal of Applied Physics, 2006, 45, 2128-2131.	1.5	16
80	Numerical investigation of the transport phenomena occurring in the growth of SiC by the induction heating TSSG method. Journal of Crystal Growth, 2017, 474, 50-54.	1.5	16
81	SiGe bulk crystal as a lattice-matched substrate to GaAs for solar cell applications. Applied Physics Letters, 2000, 77, 3565-3567.	3.3	15
82	Pattern size effect on source supply process for sub-micrometer scale selective area growth by organometallic vapor phase epitaxy. Journal of Crystal Growth, 2006, 289, 89-95.	1.5	15
83	Solubility measurement of a metastable achiral crystal of sodium chlorate in solution growth. Journal of Crystal Growth, 2014, 394, 106-111.	1.5	15
84	Plasmonic Heating-Assisted Laser-Induced Crystallization from a NaClO ₃ Unsaturated Mother Solution. Crystal Growth and Design, 2017, 17, 809-818.	3.0	15
85	In-situ monitoring system of the position and temperature at the crystal–solution interface. Journal of Crystal Growth, 2002, 236, 125-131.	1.5	14
86	Structural properties of directionally grown polycrystalline SiGe for solar cells. Journal of Crystal Growth, 2005, 275, 467-473.	1.5	14
87	Surface Morphology and Threading Dislocation Conversion Behavior during Solution Growth of 4H-SiC Using Al-Si Solvent. Materials Science Forum, 0, 778-780, 67-70.	0.3	14
88	Application of C-face dislocation conversion to 2 inch SiC crystal growth on an off-axis seed crystal. CrystEngComm, 2019, 21, 7260-7265.	2.6	14
89	Numerical investigation of the effect of static magnetic field on the TSSG growth of SiC. Journal of Crystal Growth, 2018, 498, 140-147.	1.5	14
90	Stacked Ge islands for photovoltaic applications. Science and Technology of Advanced Materials, 2003, 4, 367-370.	6.1	13

#	Article	IF	CITATIONS
91	Phase diagram of growth mode for the SiGe/Si heterostructure system with misfit dislocations. Journal of Crystal Growth, 2004, 260, 372-383.	1.5	13
92	Dislocation Conversion During SiC Solution Growth for High-Quality Crystals. Materials Science Forum, 0, 821-823, 3-8.	0.3	13
93	Septin Interferes with the Temperature-Dependent Domain Formation and Disappearance of Lipid Bilayer Membranes. Langmuir, 2016, 32, 12823-12832.	3.5	13
94	Morphology of AlN whiskers grown by reacting N2 gas and Al vapor. Journal of Crystal Growth, 2017, 468, 576-580.	1.5	13
95	Phase diagram calculation for epitaxial growth of GalnAs on InP considering the surface, interfacial and strain energies. Journal of Crystal Growth, 2000, 220, 413-424.	1.5	12
96	Molten metal flux growth and properties of CrSi2. Journal of Alloys and Compounds, 2004, 383, 319-321.	5.5	12
97	Effect of Li doping on photoluminescence from Er, O-codoped GaAs. Journal of Crystal Growth, 2007, 298, 69-72.	1.5	12
98	Effects of defects and local thickness modulation on spin-polarization in photocathodes based on GaAs/GaAsP strained superlattices. Journal of Applied Physics, 2010, 108, 094509.	2.5	12
99	4H-SiC Growth from Si-Cr-C Solution under Al and N Co-Doping Conditions. Materials Science Forum, 0, 821-823, 9-13.	0.3	12
100	Assessing composition gradient energy effects due to spin interaction on the spinodal decomposition of Fe–Cr. Materials Science & Engineering A: Structural Materials: Properties, Microstructure and Processing, 2001, 312, 128-135.	5.6	11
101	Growth of SixGe1-x(\$x allingdotseq 0.15\$) Bulk Crystal with Uniform Composition Utilizingin situMonitoring of the Crystal-solution Interface. Japanese Journal of Applied Physics, 2001, 40, 4141-4144.	1.5	11
102	Local Concentration of Gel Phase Domains in Supported Lipid Bilayers under Light Irradiation in Binary Mixture of Phospholipids Doped with Dyes for Photoinduced Activation. Langmuir, 2008, 24, 10974-10980.	3.5	11
103	Forming two-dimensional structure of DNA-functionalized Au nanoparticles via lipid diffusion in supported lipid bilayers. Journal of Crystal Growth, 2014, 401, 494-498.	1.5	11
104	Control of Macroscopic Absorption Coefficient of Multicrystalline SiGe by Microscopic Compositional Distribution. Japanese Journal of Applied Physics, 2002, 41, L37-L39.	1.5	10
105	Fabrication of SiGe-on-insulator by rapid thermal annealing of Ge on Si-on-insulator substrate. Applied Surface Science, 2004, 224, 95-98.	6.1	10
106	Size uniformity of InAs dots on mesa-structure templates on (001) InP substrates grown by droplet metal-organic vapor phase epitaxy method. Applied Physics Letters, 2006, 89, 083110.	3.3	10
107	Direct Growth of AlN Single Crystal on Sapphire by Solution Growth Method. Japanese Journal of Applied Physics, 2013, 52, 08JE17.	1.5	10
108	Increase in the Growth Rate by Rotating the Seed Crystal at High Speed during the Solution Growth of SiC. Materials Science Forum, 2014, 778-780, 63-66.	0.3	10

#	Article	IF	CITATIONS
109	In Situ Observation of Chiral Symmetry Breaking in NaClO ₃ Chiral Crystallization Realized by Thermoplasmonic Micro-Stirring. Crystal Growth and Design, 2018, 18, 4230-4239.	3.0	10
110	Development of angle-resolved spectroscopy system of electrons emitted from a surface with negative electron affinity state. Review of Scientific Instruments, 2018, 89, 073103.	1.3	10
111	Chiral Optical Force Generated by a Superchiral Near-Field of a Plasmonic Triangle Trimer as Origin of Giant Bias in Chiral Nucleation: A Simulation Study. Journal of Physical Chemistry C, 2021, 125, 6209-6221.	3.1	10
112	Synchrotron X-ray topographic image contrast variation of screw-type basal plane dislocations located at different depths below the crystal surface in 4H-SiC. Acta Materialia, 2021, 208, 116746.	7.9	10
113	Data-Driven Optimization and Experimental Validation for the Lab-Scale Mono-Like Silicon Ingot Growth by Directional Solidification. ACS Omega, 2022, 7, 6665-6673.	3.5	10
114	Evidence of the Presence of Built-in Strain in Multicrystalline SiGe with Large Compositional Distribution. Japanese Journal of Applied Physics, 2002, 41, 4462-4465.	1.5	9
115	Effects of vicinal steps on the island growth and orientation of epitaxially grown perylene-3,4,9,10-tetracarboxylic dianhydride (PTCDA) thin film crystals on a hydrogen-terminated Si(111) substrate. Journal of Crystal Growth, 2005, 273, 594-602.	1.5	9
116	Effect of Surface Polarity on the Conversion of Threading Dislocations in Solution Growth. Materials Science Forum, 0, 740-742, 15-18.	0.3	9
117	Direct observation of stacking fault shrinkage in 4H-SiC at high temperatures by <i>in-situ</i> X-ray topography using monochromatic synchrotron radiation. Applied Physics Letters, 2018, 113, .	3.3	9
118	Optimal Control of SiC Crystal Growth in the RF-TSSG System Using Reinforcement Learning. Crystals, 2020, 10, 791.	2.2	9
119	<i>In-operando</i> x-ray topography analysis of SiC metal–oxide–semiconductor field-effect transistors to visualize stacking fault expansion motions dynamically during operations. Journal of Applied Physics, 2021, 130, .	2.5	9
120	Effect of nonlinearity of the evolution equation on the spinodal decomposition process in alloys. Physical Review B, 1998, 58, 11371-11376.	3.2	8
121	Thickness dependence of stable structure of the Stranski–Krastanov mode in the GaPSb/GaP system. Journal of Crystal Growth, 2000, 209, 637-647.	1.5	8
122	Fabrication of SiGe-on-Insulator through Thermal Diffusion of Ge on Si-on-Insulator Substrate. Japanese Journal of Applied Physics, 2003, 42, L232-L234.	1.5	8
123	Supported lipid bilayer membranes on SiO 2 and TiO 2 : substrate effects on membrane formation and shape transformation. , 2007, , .		8
124	Change in Surface Morphology by Addition of Impurity Elements in 4H-SiC Solution Growth with Si Solvent. Materials Science Forum, 0, 821-823, 14-17.	0.3	8
125	Effect of magnesium ion concentration on two-dimensional structure of DNA-functionalized nanoparticles on supported lipid bilayer. Japanese Journal of Applied Physics, 2016, 55, 03DF11.	1.5	8
126	Molecular beam epitaxy of GaAs on nearly lattice-matched SiGe substrates grown by the multicomponent zone-melting method. Semiconductor Science and Technology, 2001, 16, 699-703.	2.0	7

#	Article	IF	CITATIONS
127	Simultaneous in situ measurement of solute and temperature distributions in the alloy solutions. Journal of Crystal Growth, 2002, 242, 313-320.	1.5	7
128	Fabrication of solar cell with stacked Ge islands for enhanced absorption in the infrared regime. Thin Solid Films, 2004, 451-452, 604-607.	1.8	7
129	Effects of growth temperature on the surface morphology of silicon thin films on (111) silicon monocrystalline substrate by liquid phase epitaxy. Journal of Crystal Growth, 2004, 266, 467-474.	1.5	7
130	Improvement of Surface Morphology by Solution Flow Control in Solution Growth of SiC on Off-Axis Seeds. Materials Science Forum, 0, 821-823, 31-34.	0.3	7
131	Thin film growth of CaFe2As2by molecular beam epitaxy. Superconductor Science and Technology, 2016, 29, 015013.	3.5	7
132	Plasmonic Manipulation of Sodium Chlorate Chiral Crystallization: Directed Chirality Transfer via Contact-Induced Polymorphic Transformation and Formation of Liquid Precursor. Crystal Growth and Design, 2020, 20, 5493-5507.	3.0	7
133	Explainable machine learning for the analysis of transport phenomena in top-seeded solution growth of SiC single crystal. Journal of Thermal Science and Technology, 2021, 16, JTST0009-JTST0009.	1.1	7
134	Solvent design aiming at solution property induced surface stability: A case study using SiC solution growth. Journal of Crystal Growth, 2022, 578, 126425.	1.5	7
135	In SituMeasurement of Composition in High-Temperature Solutions by X-Ray Fluorescence Spectrometry. Japanese Journal of Applied Physics, 2000, 39, 5981-5982.	1.5	6
136	High-Quality Crystalline Silicon Layer Grown by Liquid Phase Epitaxy Method at Low Growth Temperature. Japanese Journal of Applied Physics, 2003, 42, L217-L219.	1.5	6
137	Effects of absorbed group-V atoms on the size distribution and optical properties of InAsP quantum dots fabricated by the droplet hetero-epitaxy. Journal of Crystal Growth, 2008, 310, 2239-2243.	1.5	6
138	Epitaxial growth of LaFeAs(O,F) thin films by molecular beam epitaxy. Physica C: Superconductivity and Its Applications, 2011, 471, 1174-1176.	1.2	6
139	Defect Evaluation of SiC Crystal Grown by Solution Method: The Study by Synchrotron X-Ray Topography and Etching Method. Materials Science Forum, 2011, 679-680, 28-31.	0.3	6
140	Stable Growth of 4H-SiC Single Polytype by Controlling the Surface Morphology Using a Temperature Gradient in Solution Growth. Materials Science Forum, 0, 717-720, 53-56.	0.3	6
141	Phase-locking of oscillating images using laser-induced spin-polarized pulse TEM. Microscopy (Oxford,) Tj ETQq1	1 0.7843 1.5	14 rgBT /Ove
142	Bulk 3C-SiC Crystal by Top Seeded Solution Growth Method. Materials Science Forum, 0, 740-742, 311-314.	0.3	6
143	Characterization of V-Shaped Defects Formed during the 4H-SiC Solution Growth by Transmission Electron Microscopy and X-ray Topography Analysis. Crystal Growth and Design, 2016, 16, 5136-5140.	3.0	6
144	Dislocation Behavior in Bulk Crystals Grown by TSSG Method. Materials Science Forum, 0, 924, 39-42.	0.3	6

#	Article	IF	CITATIONS
145	Adjoint-based sensitivity analysis for the optimal crucible temperature profile in the RF-Heating TSSC-SiC crystal growth process. Journal of Crystal Growth, 2019, 517, 59-63.	1.5	6
146	The Prediction Model of Crystal Growth Simulation Built by Machine Learning and Its Applications. Vacuum and Surface Science, 2019, 62, 136-140.	0.1	6
147	Temperature dependence of double Shockley stacking fault behavior in nitrogen-doped 4H-SiC studied by in-situ synchrotron X-ray topography. Acta Materialia, 2020, 194, 387-393.	7.9	6
148	Ordered Arrangement of Planar Faults with Picoscale Perfection in Titanium Oxide Natural Superlattices. Journal of Physical Chemistry C, 2021, 125, 11175-11181.	3.1	6
149	Numerical investigation of solute evaporation in crystal growth from solution: A case study of SiC growth by TSSG method. Journal of Crystal Growth, 2022, 579, 126448.	1.5	6
150	Fabrication of SiGe bulk crystals with uniform composition as substrates for Si-based heterostructures. Materials Science and Engineering B: Solid-State Materials for Advanced Technology, 2002, 89, 364-367.	3.5	5
151	Crystal Quality Evaluation of 6H-SiC Layers Grown by Liquid Phase Epitaxy around Micropipes using Micro-Raman Scattering Spectroscopy. Materials Science Forum, 2004, 457-460, 633-636.	0.3	5
152	Growth of InGaAs and SiGe homogeneous bulk crystals which have complete miscibility in the phase diagrams. International Journal of Materials and Product Technology, 2005, 22, 185.	0.2	5
153	Growth of SiC Single Crystal from Si-C-(Co, Fe) Ternary Solution. Materials Science Forum, 2006, 527-529, 115-118.	0.3	5
154	Temperature dependence of carrier relaxation time in gallium phosphide evaluated by photoemission measurements. AIP Advances, 2017, 7, 115314.	1.3	5
155	The Effect of Crucible Rotation and Crucible Size in Topâ€Seeded Solution Growth of Singleâ€Crystal Silicon Carbide. Crystal Research and Technology, 2019, 54, 1900014.	1.3	5
156	Control of microstructure and mechanical properties of sintered aluminum nitride through addition of aluminum nitride whiskers. Journal of Asian Ceramic Societies, 2021, 9, 1248-1254.	2.3	5
157	Nucleation sites of expanded stacking faults detected by <i>in operando</i> x-ray topography analysis to design epitaxial layers for bipolar-degradation-free SiC MOSFETs. AIP Advances, 2022, 12, .	1.3	5
158	Evaluation of the diffusion coefficients in liquid GaGe binary alloys using a novel method based on Fick's first law. Journal of Non-Crystalline Solids, 2002, 312-314, 196-202.	3.1	4
159	Solution Growth of SiC Crystals in Si-Ti and Si-Ge-Ti Solvents. Materials Science Forum, 0, 600-603, 59-62.	0.3	4
160	Stability Growth Condition for 3C-SiC Crystals by Solution Technique. Materials Science Forum, 2008, 600-603, 63-66.	0.3	4
161	Polytype and Crystal Quality of SiC Crystals Grown on 3C-SiC by Seeded Solution Method. Materials Science Forum, 2009, 615-617, 27-30.	0.3	4
162	Development of Spin-Polarized Pulsed TEM. Journal of Physics: Conference Series, 2012, 371, 012004.	0.4	4

#	Article	IF	CITATIONS
163	Effect of Forced Convection by Crucible Design in Solution Growth of SiC Single Crystal. Materials Science Forum, 0, 821-823, 22-25.	0.3	4
164	Research on Solvent Composition for Different Surface Morphology on C Face during 4H-SiC Solution Growth. Materials Science Forum, 0, 821-823, 39-42.	0.3	4
165	Polytype control by activity ratio of silicon to carbon during SiC solution growth using multicomponent solvents. Japanese Journal of Applied Physics, 2016, 55, 01AC01.	1.5	4
166	High-Temperature Solution Growth and Characterization of Chromium Disilicide. Japanese Journal of Applied Physics, 2003, 42, 7292-7293.	1.5	3
167	Growth of SiGe-on-insulator and its application as a substrate for epitaxy of strained-Si layer. Journal of Crystal Growth, 2005, 275, e1203-e1207.	1.5	3
168	Shape Transformation of Adsorbed Vesicles on Oxide Surfaces: Effect of Substrate Material and Photo-Irradiation. Transactions of the Materials Research Society of Japan, 2009, 34, 183-188.	0.2	3
169	Polytype Stability of 4H-SiC Seed Crystal on Solution Growth. Materials Science Forum, 0, 679-680, 24-27.	0.3	3
170	Analysis of thickness modulation in GaAs/GaAsP strained superlattice by TEM observation. Journal of Crystal Growth, 2012, 353, 84-87.	1.5	3
171	Growth of a smooth CaF2layer on NdFeAsO thin film. Journal of Physics: Conference Series, 2014, 507, 012047.	0.4	3
172	Control of Interface Shape by Non-Axisymmetric Solution Convection in Top-Seeded Solution Growth of SiC Crystal. Materials Science Forum, 2015, 821-823, 18-21.	0.3	3
173	Influences of Solution Flow and Lateral Temperature Distribution on Surface Morphology in Solution Growth of SiC. Materials Science Forum, 0, 821-823, 35-38.	0.3	3
174	Suppression of Polytype Transformation with Extremely Low-Dislocation-Density 4H-SiC Crystal in Two-Step Solution Method. Materials Science Forum, 0, 924, 60-63.	0.3	3
175	In Situ Microscopic Observation on Surface Kinetics in Optical Trapping-Induced Crystal Growth: Step Formation, Wetting Transition, and Nonclassical Growth. Crystal Growth and Design, 2019, 19, 4138-4150.	3.0	3
176	Numerical Study of Three-Dimensional Melt Flows during the TSSG Process of SiC Crystal for the Influence of Input Parameters of RF-Coils and an External Rotating Magnetic Field. Crystals, 2020, 10, 111.	2.2	3
177	Two-Step Nanoparticle Crystallization via DNA-Guided Self-Assembly and the Nonequilibrium Dehydration Process. Crystal Growth and Design, 2021, 21, 4506-4515.	3.0	3
178	Optimization of Flow Distribution by Topological Description and Machine Learning in Solution Growth of SiC. Advanced Theory and Simulations, 2022, 5, .	2.8	3
179	The excess free energy due to the composition gradient for ferromagnetic alloys. Acta Materialia, 1999, 47, 3041-3048.	7.9	2
180	Strain distribution of Si thin film grown on multicrystalline-SiGe with microscopic compositional distribution. Journal of Applied Physics, 2002, 92, 7098-7101.	2.5	2

#	Article	IF	CITATIONS
181	Relationship between Device Performance and Grain Boundary Structural Configuration in a Solar Cell Based on Multicrystalline SiGe. Japanese Journal of Applied Physics, 2004, 43, L250-L252.	1.5	2
182	Electron spectroscopy of conduction electrons excited by visible light utilizing NEA surface. , 2013, , .		2
183	Immobilization of partial dislocations bounding double Shockley stacking faults in 4H-SiC observed by in situ synchrotron X-ray topography. Materialia, 2021, 20, 101246.	2.7	2
184	Successful Growth of InxGa1-xAs (x>0.18) Single Bulk Crystal Directly on GaAs Seed Crystal with Preferential Orientation. Japanese Journal of Applied Physics, 2004, 43, L907-L909.	1.5	1
185	Influence of growth temperature on minority-carrier lifetime of Si layer grown by liquid phase epitaxy using Ga solvent. Journal of Applied Physics, 2005, 98, 073708.	2.5	1
186	Development of the New Type Polarized Electron Source for SPLEEM. AIP Conference Proceedings, 2007, , .	0.4	1
187	Desorption Time of As Adsorbed on GalnAs Surface Analyzed by X-ray CTR Scattering. Indium Phosphide and Related Materials Conference (IPRM), IEEE International Conference on, 2007, , .	0.0	1
188	Anisotropy of mosaic structure of GaAsP layers grown on GaAs substrates. Physica Status Solidi (A) Applications and Materials Science, 2009, 206, 1785-1789.	1.8	1
189	Stacking Faults around the Hetero-Interface Induced by 6H-SiC Polytype Transformation on 3C-SiC with Solution Growth. Materials Science Forum, 0, 645-648, 363-366.	0.3	1
190	Ultrahigh-resolution direct observation of mini-bands formed in InGaAs/AlGaAs superlattice. , 2013, , .		1
191	Direct measurement of conduction miniband structure in superlattice by visible-light photoemission spectroscopy. , 2014, , .		1
192	Spatial Distribution of Carrier Concentration in 4H-SiÐ; Crystal Grown by Solution Method. Materials Science Forum, 2016, 858, 57-60.	0.3	1
193	Phase transition process in DDAB supported lipid bilayer. Journal of Crystal Growth, 2017, 468, 88-92.	1.5	1
194	Strain of GaAs/GaAsP Superlattices Used as Spin-Polarized Electron Photocathodes, Determined by X-Ray Diffraction. E-Journal of Surface Science and Nanotechnology, 2010, 8, 125-130.	0.4	1
195	Shape Anisotropy of CP Zone in Early Decomposition Process of Al-Zn Binary Alloy. Nippon Kinzoku Gakkaishi/Journal of the Japan Institute of Metals, 1998, 62, 117-124.	0.4	1
196	Designing a High-Crystallinity Nano-Gapped Particle Superlattice via DNA-Guided Colloidal Crystallization and Dehydration. Crystal Growth and Design, 0, , .	3.0	1
197	Grain growth of polycrystalline Si thin film for solar cells and its effect on crystal properties. , 0, , .		0
198	Si/multicrystalline-SiGe heterostructure as a candidate for solar cells with high conversion		0

efficiency., 0, , .

#	Article	IF	CITATIONS
199	TEM Studies on the Initial Stage of Seeded Solution Growth of 6H-SiC using Metal Solvent. Materials Science Forum, 2004, 457-460, 347-350.	0.3	0
200	The Wideband Light Emission around 800 nm from Ternary InAsP Quantum Dots with an Intentionally Broadened Size and Composition Distribution. , 0, , .		0
201	2P293 Formation of domains in fluorescent lipids doped DMPC-DOPC binary bilayers supported on SiO_2/Si substrates under local light irradiation.(40. Membrane structure,Poster) Tj ETQq1 1 0.784314 rgBT /Ove	erl o ck 10 T	ſf 5 0 657 T⊲
202	Minority carrier dynamics in polycrystalline silicon solar cells studied by photo-assisted Kelvin probe force microscopy. Conference Record of the IEEE Photovoltaic Specialists Conference, 2008, , .	0.0	0
203	2P-229 In situ Observation of Molecular Diffusion in Supported Lipid Bilayer on Oxide Surfaces by Substrate-Derestricted Single-Molecule Tracking(The 46th Annual Meeting of the Biophysical Society) Tj ETQq1 1	007.84314	4 r <mark>g</mark> BT /Over
204	Effects of Applied Voltage on the Size of Phase-Separated Domains in DMPS-DOPC Lipid Binary Bilayers Supported on SiO ₂ /Si Substrates. Transactions of the Materials Research Society of Japan, 2009, 34, 217-220.	0.2	0
205	Local Condensation of Artificial Raft Domains under Light Irradiation in Supported Lipid Bilayer of PSM-DOPC-Cholesterol System. Transactions of the Materials Research Society of Japan, 2009, 34, 179-182.	0.2	0
206	High Brightness and high polarization electron source using transmission photocathode. , 2009, , .		0
207	8.5: Effects of defects and local thickness modulation on spin-polarization in photocathodes based on GaAs/GaAsP strained superlattices. , 2010, , .		0
208	Increase of spectral width of stacked InAs quantum dots on GaAs by controlling spacer layer thickness. Journal of Crystal Growth, 2011, 318, 1113-1116.	1.5	0
209	Measurement of energy distribution of conduction electrons in superlattice by visible-light photoemission spectroscopy. , 2015, , .		0
210	B11-O-14Coherences of spin-polarized and pulsed electron beam extracted from a semiconductor photocathode in TEM. Microscopy (Oxford, England), 2015, 64, i17.1-i17.	1.5	0
211	3C-SiC Crystal on Sapphire by Solution Growth Method. Materials Science Forum, 2015, 821-823, 185-188.	0.3	0
212	Semi in-situ measurement of zincate ion concentration near zinc anode using background-oriented Schlieren technique. Physical Review Research, 2019, 1, .	3.6	0
213	Design of High-quality SiC Solution Growth Condition Assisted by Machine Learning. Materia Japan, 2020, 59, 145-152.	0.1	0
214	Kuwahara etÂal. Reply:. Physical Review Letters, 2021, 127, 229602.	7.8	0